NANO · MICRO small
www.small-journal.com

Three Birds with One Stone: An Integrated Cathode–Electrolyte Structure for High-Performance Solid-State Lithium–Oxygen Batteries

*Chao-Le Li, Gang Huang, Yue Yu, Qi Xiong, Jun-Min Yan, and Xin-Bo Zhang**

Constructing solid-state lithium–oxygen batteries (SSLOBs) holds a great promise to solve the safety and stability bottlenecks faced by lithium–oxygen batteries (LOBs) with volatile and flammable organic liquid electrolytes. However, the realization of high-performance SSLOBs is full of challenges due to the poor ionic conductivity of solid electrolytes, large interfacial resistance, and limited reaction sites of cathodes. Here, a flexible integrated cathode–electrolyte structure (ICES) is designed to enable the tight connection between the cathode and electrolyte through supporting them on a 3D SiO_2 nanofibers (NFs) framework. The intimate cathode–electrolyte structure and the porous SiO_2 NFs scaffold combination are favorable for decreasing interfacial resistance and increasing reaction sites. Moreover, the 3D SiO_2 NFs framework can also behave as an efficient inorganic filler to enhance the ionic conductivity of the solid polymer electrolyte and its ability to inhibit lithium dendrite growth. As a result, the elaborately designed ICES can simultaneously tackle the issues that limit the performance liberation of SSLOBs, making the batteries deliver a high discharge capacity and a long lifetime of 145 cycles with a cycling capacity of 1000 mAh g^{-1} at 60 °C, much superior to coventional SSLOBs (50 cycles).

1. Introduction

Aprotic lithium–oxygen batteries (LOBs) have been recognized as an appealing candidate for next-generation energy storage devices owing to their ultrahigh theoretical energy density (≈3500 Wh kg^{-1}).[1–3] However, despite intensive studies have been carried out to facilitate the performance improvement of liquid-based LOBs, several serious challenges associated with the evaporation and flammability of organic liquid electrolytes, Li dendrite growth, and Li corrosion by the dissolved oxygen and moisture still remain to be addressed by a simple way.[4–7] Replacing the liquid electrolyte with solid one to build solid-state lithium–oxygen batteries (SSLOBs) is expected to solve these challenges, because the solid electrolytes (SEs) possess some particular merits that the liquid electrolyte does not easily have, like the ability of flame retardant, protecting the Li metal anode from oxygen/moisture attack, and suppressing the growth of lithium dendrites.[8–12] However, the use of SEs would encounter new issues, such as the low ionic conductivity of SEs at room temperature, poor solid–solid physical contact between the SE and electrode, and the discontinuous Li^+/e^- transport pathways in the cathode, which severely hinder the SSLOBs to deliver high electrochemical performance. In addition, the technique for large-scale production of SEs remains to be developed.[12] Therefore, it is vital to develop a method to solve these challenges to make the SSLOBs realize performance improvement that is closer to real-world implementation.

Different from the rigid inorganic solid electrolytes, the flexible solid polymer electrolytes (SPEs) are convenient for mass preparation, but their low ionic conductivity impedes them from constructing high-performance SSLOBs.[12,13] It has been demonstrated that the introduction of ceramic fillers into the SPE to fabricate composite solid electrolyte (CSE) could improve the ionic conductivity to some extent, but most of the work uses nanoparticle-type fillers that cannot form a continuous network and avoid the particle agglomeration, which limits the further improvement of the Li^+ conductivity.[14–18] To this end, ceramic fillers with a 3D structure emerge to eliminate these disadvantages and establish a long-range continuous interface with the polymer matrix.[19–21] Despite promising, the current 3D ceramic fillers have poor flexibility and complex preparation processes, and a general and straightforward strategy is highly needed to promote their functional applications. Solving the low Li^+ conductivity conundrum of CSE by 3D flexible fillers still cannot guarantee a high-performance SSLOB, which then makes us move to address the large interfacial resistance issue between the independent SE and electrode. This could be realized by enhancing the

C.-L. Li, Q. Xiong, J.-M. Yan
Key Laboratory of Automobile Materials
Ministry of Education
Department of Materials Science and Engineering
Jilin University
Changchun 130022, P. R. China
C.-L. Li, G. Huang, Y. Yu, Q. Xiong, X.-B. Zhang
State Key Laboratory of Rare Earth Resource Utilization
Changchun Institute of Applied Chemistry
Chinese Academy of Sciences
Changchun 130022, P. R. China
E-mail: xbzhang@ciac.ac.cn
The ORCID identification number(s) for the author(s) of this article can be found under https://doi.org/10.1002/smll.202107833.

DOI: 10.1002/smll.202107833

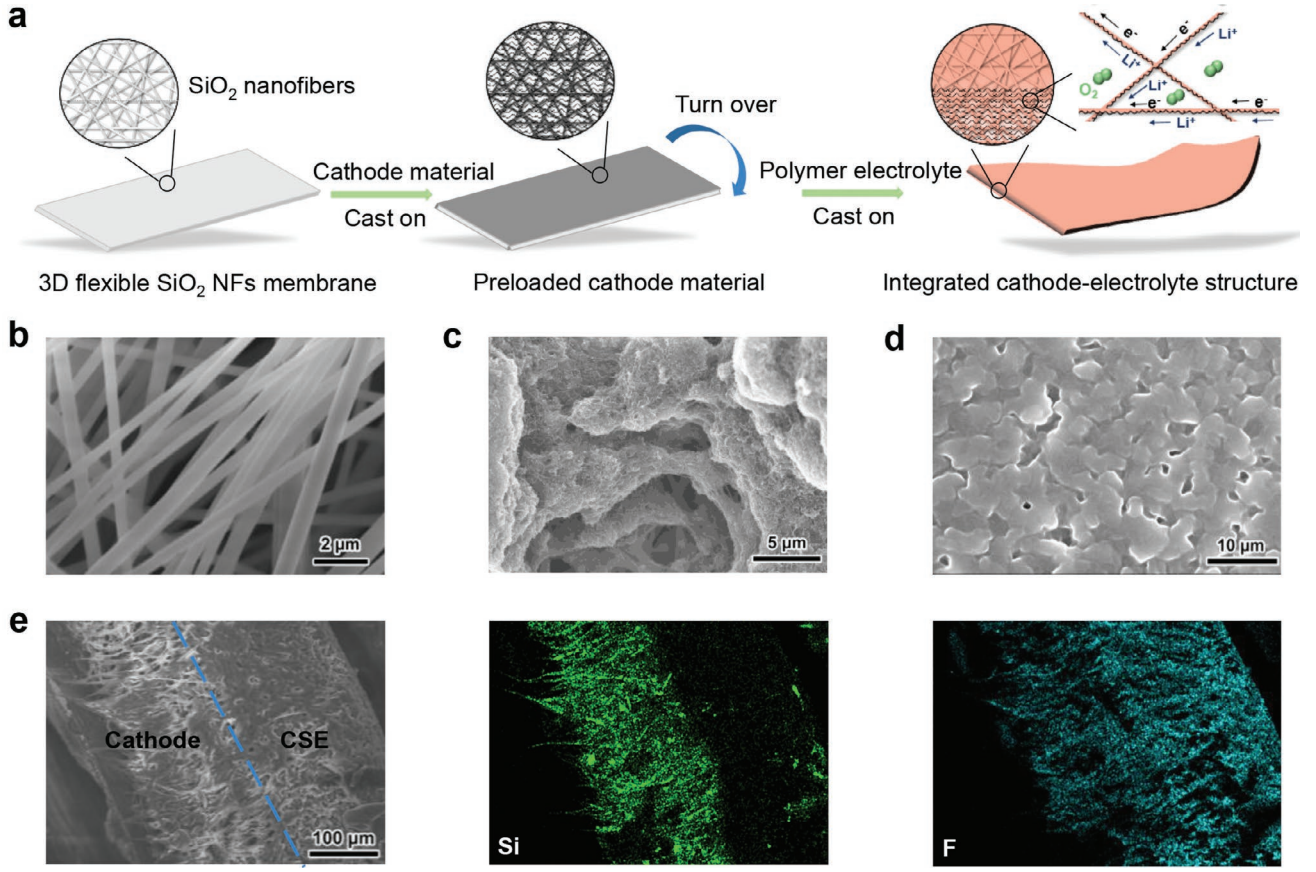

Figure 1. a) Schematic of the preparation process of the ICES with 3D SiO_2 NFs membrane as a supporting framework. The integrated structure is composed of a dense CSE layer and a porous cathode layer. SEM images of b) SiO_2 NFs, c) porous cathode side, and d) CSE side. e) Cross-sectional SEM image and corresponding EDS mappings of the ICES.

electrode–electrolyte interfacial contact and adhesion just as the solid-state lithium–ion batteries (SSLIBs) do through completely filling the cathode with a polymer electrolyte to form a relatively dense structure.[22] Nevertheless, this approach does not work well for SSLOBs when considering their semi-open feature. The cathode for SSLOBs requires suitable pores to promote oxygen diffusion and provide sufficient space to accommodate the discharge products.[23] Besides the porous structure, the cathode should also have continuous Li^+ and electron transport channels to form abundant three-phase (e^-, Li^+, O_2) boundaries to act as reaction sites for facilitating the oxygen reduction/evolution reaction.[24] However, since the nonflowing characteristic of the SE makes the interfacial contact between the SE and cathode is rather finite, the reaction sites in SSLOBs are much lower than those in liquid-based LOBs, in which the electrolyte could wet the whole cathode. Even though the limitation is explicit, to date, there is still no solution that could effectively conquer it. And most of the cathodes for SSLOBs are prepared by simply mixing the SE and carbon material, and then sintering on the inorganic solid electrolyte pellet to increase the electrode–electrolyte contact area.[25] Whereas, the increase is still far from the demands that could enable a high-performance SSLOB. It is necessary to design a convenient and valid strategy to simultaneously improve the ionic conductivity of SPE, decrease the interfacial resistance, and construct rich reaction sites in the cathode to make the SSLOBs achieve significant performance amelioration.

Here, we have proposed a new design concept of using 3D SiO_2 nanofibers (NFs) membrane as a supporting framework to construct a flexible integrated cathode–electrolyte structure (ICES) for SSLOBs (**Figure 1**a). In this configuration, the self-standing 3D SiO_2 NFs framework is the key component that not only acts as a bridge to connect the CSE and cathode, but also serves as a 3D ceramic filler and porous cathode support to increase the ionic conductivity of the SPE and the reaction sites in the cathode. Moreover, unlike the conventional independent cathode and electrolyte structure in previous SSLOBs, the CSE and cathode in the designed integrated structure share the same framework and interconnect with each other, reducing the interfacial resistance with a small battery polarization. Importantly, the CSE side of the integrated structure could also assure its firm contact with the Li metal anode and its ability to inhibit the growth of lithium dendrites. As a result, the SSLOBs with the ICES present a high discharge capacity, good rate capability, and a long cycle lifetime. Meanwhile, the assembled pouch-type SSLOBs exhibit excellent flexibility and high-level safety.

2. Results and Discussion

SiO_2 NFs framework was first prepared by a simple electrospinning method and followed by a high-temperature calcination process. The as-prepared free-standing SiO_2 NFs membrane with an amorphous feature exhibits good flexibility and can be freely bent (Figures S1 and S2, Supporting Information). The scanning electron microscopy (SEM) image of the SiO_2 NFs shows that they have an average diameter of 450 nm, and the nanofibers form a 3D network structure (Figure 1b; and Figure S3, Supporting Information). The peaks at 1070 and 803 cm^{-1} in the Fourier transform infrared spectroscopy (FTIR) can be assigned to the characteristic peaks of SiO_2, confirming the successful synthesis of SiO_2 NFs (Figure S4, Supporting Information).[26,27] After getting the SiO_2 NFs framework, the cathode slurry was cast on its one side to preload the cathode material. The SEM image reveals that the interconnected Ru/CNT is well attached to the SiO_2 NFs with plenty of pores remaining (Figure 1c; and Figure S5, Supporting Information). Then, the poly(vinylidene fluoride-*co*-hexafluoropropylene) (PVDF-HFP)/bis(trifluoromethane)sulfonimide lithium (LiTFSI) SPE was cast on the other side of the SiO_2 NFs skeleton to form a CSE, thus getting a SiO_2 NFs supported ICES (Figure 1a). As shown in Figure 1d, the SiO_2 NFs in the electrolyte side are buried by the SPE and they cannot be discerned at the top layer. In the ICES, the CSE layer and the porous cathode layer share the same 3D SiO_2 NFs framework; therefore, they form an integrated structure with tight contact, as shown in the cross-section SEM image of the ICES and its corresponding energy-dispersive X-ray spectroscopy (EDS) images (Figure 1e). The EDS points out that the Si element is mainly concentrated on the cathode side, while the F element is dispersed in the entire integrated structure. Considering the Si and F elements belong to SiO_2 NFs and PVDF-HFP polymer electrolytes, respectively, the inconspicuous detectable Si element in the dense CSE can be ascribed to the well cover of SiO_2 NFs by the PVDF-HFP polymer electrolyte (Figure 1d; and Figure S6, Supporting Information). For the cathode side, the porous structure is still maintained with discernible SiO_2 NFs after the introduction of the SPE; consequently, the Si element could be detected. The thicknesses of the CSE layer and the porous layer are both around 200 µm (Figure 1e). It is worth noting that the diffusion of the SPE to the cathode side increases their intimate interfacial contact area, which guarantees the rapid transfer of Li^+

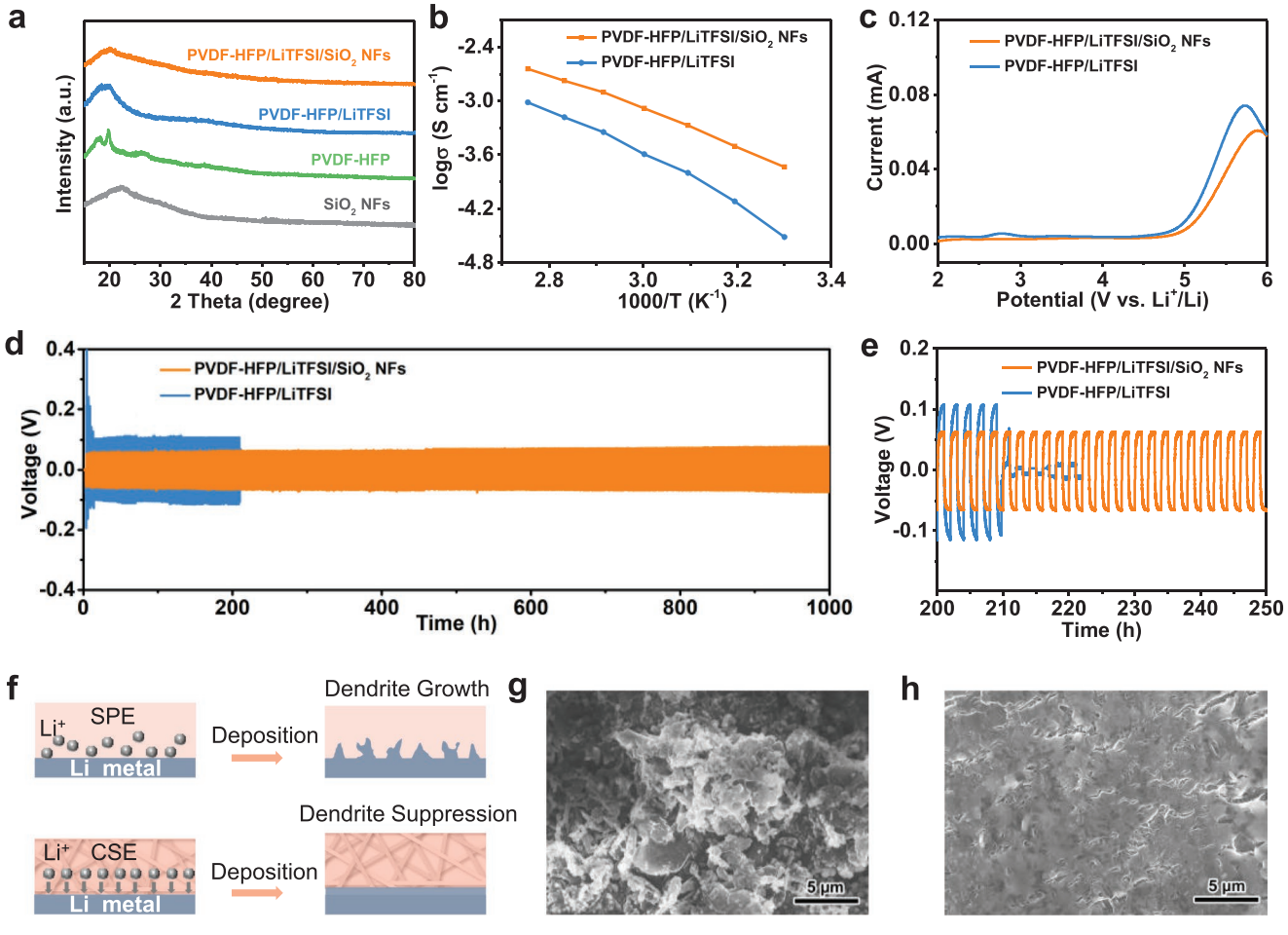

Figure 2. a) XRD patterns of SiO_2 NFs, PVDF-HFP, PVDF-HFP/LiTFSI SPE, and PVDF-HFP/LiTFSI/SiO_2 NFs CSE. b) Ionic conductivities of SPE and CSE at different temperatures. c) LSV curves of SPE and CSE at a scan rate of 5 mV s^{-1}. d) Voltage profiles of the Li/Li symmetric cells at a current density of 0.1 mA cm^{-2}, and e) zoom-in voltage profiles between 200 and 250 h. f) Schematic illustrations of the Li deposition behavior with SPE and CSE. SEM images of the cycled Li metal electrodes with g) SPE and h) CSE.

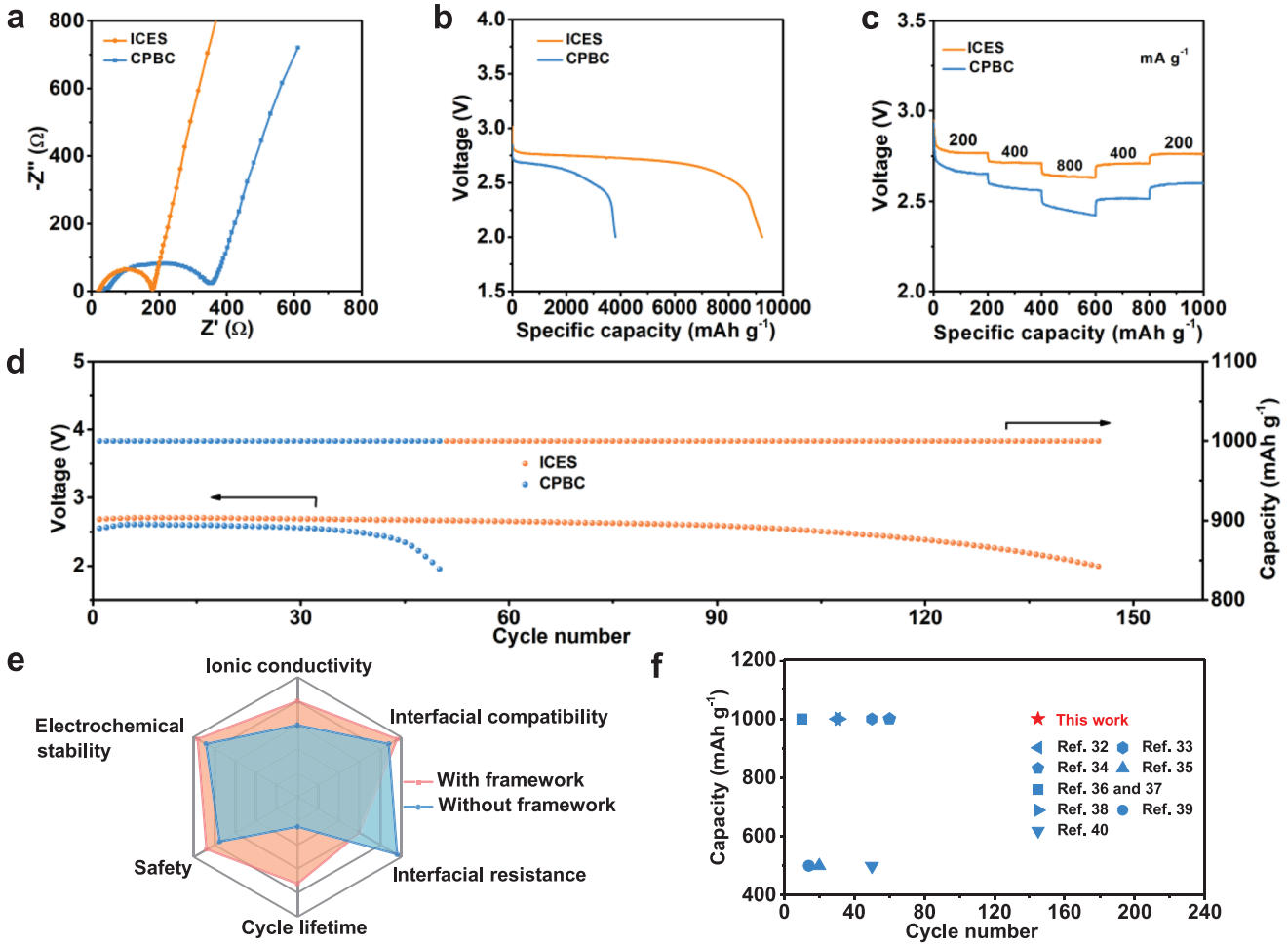

Figure 3. The electrochemical performance of SSLOBs at 60 °C. a) EIS of the SSLOBs with CPBC and ICES. b) Full discharge curves of the SSLOBs with CPBC and ICES. c) Rate performance of the SSLOBs. d) Cycling performance of the SSLOBs at a limited capacity of 1000 mAh g^{-1} and a current density of 500 mA g^{-1}. e) Radar chart of the characteristics of the electrolytes or SSLOBs with and without SiO_2 NFs framework. f) Comparison of the cycling lifetime of the ICES-based SSLOBs with previous reported results.

on these interfaces. At the cathode of ICES, the preloaded Ru/CNT forms a continuous electron transfer network, the entered polymer electrolyte provides efficient Li^+ transport pathways, and the remaining porous structure allows oxygen to be efficiently transmitted (Figure 1a; and Figure S7, Supporting Information), making the cathode with rich reaction sites (Li^+, e^-, O_2) with the help of the 3D SiO_2 NFs supporting framework.

To study the properties of the CSE layer in the integrated structure, both sides of the SiO_2 NFs framework were cast with the SPE to prepare independent CSEs. **Figure 2**a gives the XRD patterns of the PVDF-HFP, PVDF-HFP/LiTFSI SPE, and PVDF-HFP/LiTFSI/SiO_2 NFs CSE. The diffraction peaks of the PVDF-HFP used here corresponds to the α-phase PVDF-HFP.[28,29] With the addition of LiTFSI salt, the peak intensity for PVDF-HFP decreases, and the introduction of SiO_2 NFs skeleton further weakens the peaks, that is, significantly decreases the crystallinity of PVDF-HFP, which is beneficial to the migration of Li^+ ion.[30] The ionic conductivity of the CSE was measured by electrochemical impedance spectroscopy (EIS) to check the resistance of the battery that sandwiches CSE between two stainless steel sheets. It is calculated that the CSE has a Li^+ conductivity of 1.82×10^{-4} S cm^{-1} at room temperature, while the value for SPE (3.10×10^{-5} S cm^{-1}) is an order of magnitude lower than the CSE, indicating that the introduction of the SiO_2 NFs skeleton could certainly improve the ionic conductivity of the CSE. This ionic conductivity increase could be attributed to the SiO_2 NFs induced crystallinity decrease of the polymer, and the facile dissociation of the lithium salt by the interaction between SiO_2 NFs and the polymer matrix.[30,31] Figure 2b exhibits the temperature-dependent ionic conductivities of the solid electrolytes in the temperature range of 30–90 °C. We can see that the ionic conductivities of the SPE and CSE increase with the rise of temperature, and the ionic conductivity of CSE is always higher than that of SPE at the same temperature. In addition to the high ionic conductivity, the CSE also possesses a wider electrochemical stability window than the SPE (4.8 vs 4.5 V, Figure 2c), suggesting that the CSE could to some extent resist the high voltage rendered electrolyte decomposition. The thermal stability of the CSE was examined by thermogravimetric analysis (TGA) (Figure S8, Supporting Information). There is only a slight mass loss for the CSE before 200 °C due to the removement of the absorbed moisture and residual solvent.

Importantly, the CSE with around 11 wt% SiO_2 NFs shows good thermal stability with a decomposition temperature up to 250 °C. In addition, the tensile strength of the CSE is higher than that of the SPE (6.68 vs 4.35 MPa, Figure S9, Supporting Information). This strong mechanical strength of CSE is beneficial to inhibit the dendrite growth on the Li anode side. The 3D SiO_2 NFs supporting framework enabled high ionic conductivity and improved electrochemical, thermal, and mechanical stability of the CSE are all essentials to make the SSLOBs realize stable operation, and none of them can be dispensed.

To investigate the dendrite suppression ability of the SEs, Li/Li symmetrical cells were assembled and measured at a current density of 0.1 mA cm^{-2} (Figure 2d,e). For Li/SPE/Li symmetrical cell, it is short-circuited with a sudden voltage drop after only 210 h cycling. In contrast, the Li/CSE/Li symmetrical cell presents much lower overpotentials and longer cycle lifetime (1000 h) than the Li/SPE/Li cell, manifesting that the CSE could not only facilitate the Li plating/stripping, but also effectively inhibit the growth of lithium dendrites (Figure 2f). In order to further confirm the enhanced dendrite suppression ability of the CSE, the morphologies of the Li electrodes after cycling in symmetric cells were investigated. Unlike the obvious irregular Li dendrites on the Li electrode surface in the Li/SPE/Li cell, the surface of the Li electrode in the Li/CSE/Li cell exhibits smooth and compact morphology without discernible dendrites (Figure 2g,h; and Figure S10, Supporting Information), demonstrating that the SiO_2 NFs framework improves the ability to suppress Li dendrite growth.

After confirming the advantages of the ICES, SSLOBs were assembled to check its working functionalities in actual batteries. Nonintegrated SSLOBs with separated CSE membrane and carbon paper-based cathode (CPBC) were also assembled for comparison. The EIS of the SSLOBs with different cathode–electrolyte structures is shown in **Figure 3**a. It can be seen that both the cell resistance and the charge transfer resistance of the ICES-based SSLOB are much lower than those of the CPBC-based SSLOB. The large interfacial contact area, tight connection between electrode and electrolyte in the ICES, and the improved Li^+ conductivity together contribute to the decreased resistance of the ICES-based SSLOB. However, for CPBC-based SSLOB, the CSE and the cathode are independent with poor physical contact and wettability, resulting in a limited contact area and consequently a large resistance.

Figure 3b gives the 1st cycle full discharge voltage curves of the SSLOBs with different cathode–electrolyte structures at 200 mA g^{-1} and 60 °C. The ICES-based SSLOB with high discharge voltages exhibits a large discharge capacity of 9220 mAh g^{-1}, more than two times that of the CPBC-based SSLOB (3812 mAh g^{-1}). This significant capacity increase for the ICES-based SSLOB is predominantly attributed to the low interfacial resistance and rich reaction sites of the ICES. Furthermore, the ICES-based SSLOB also delivers a much better rate capability with constantly higher discharge voltages than the CPBC-based SSLOB at different current densities (Figure 3c). Then, the cycling performance of the SSLOBs was studied. As shown in Figure 3d, the SSLOB with ICES can stably operate up to 145 cycles with a limited capacity of 1000 mAh g^{-1} at 500 mA g^{-1}, while the battery with CPBC can only run 50 cycles (Figures S11 and S12, Supporting Information). These results certify that the superior qualities of the ICES could be well reflected in the battery performance improvement (Figure 3e). It is worth noting that the achieved lifetime of the ICES-based SSLOB is much better than

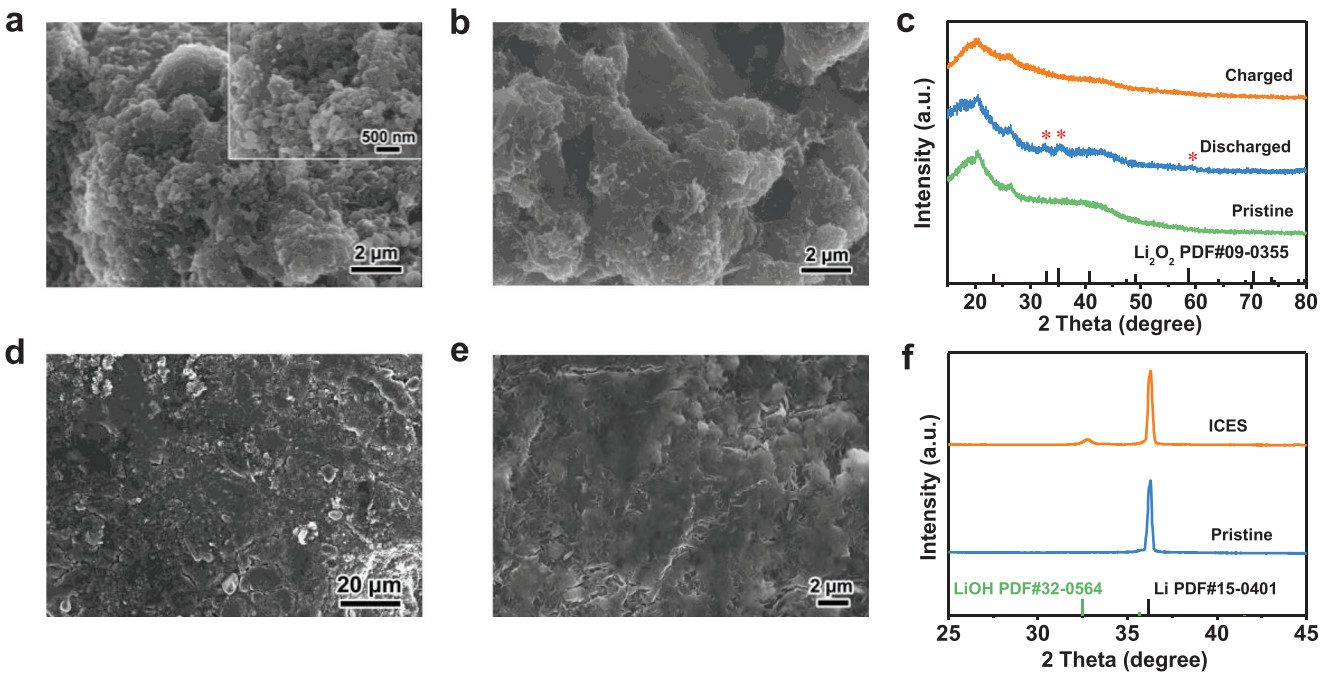

Figure 4. SEM images of the cathodes after first a) discharge and b) recharge processes. c) XRD patterns of the pristine, discharged, and recharged cathodes. d,e) SEM images of the cycled Li anode in ICES-based SSLOBs. f) XRD patterns of the pristine Li anode and the Li anode after cycling with ICES.

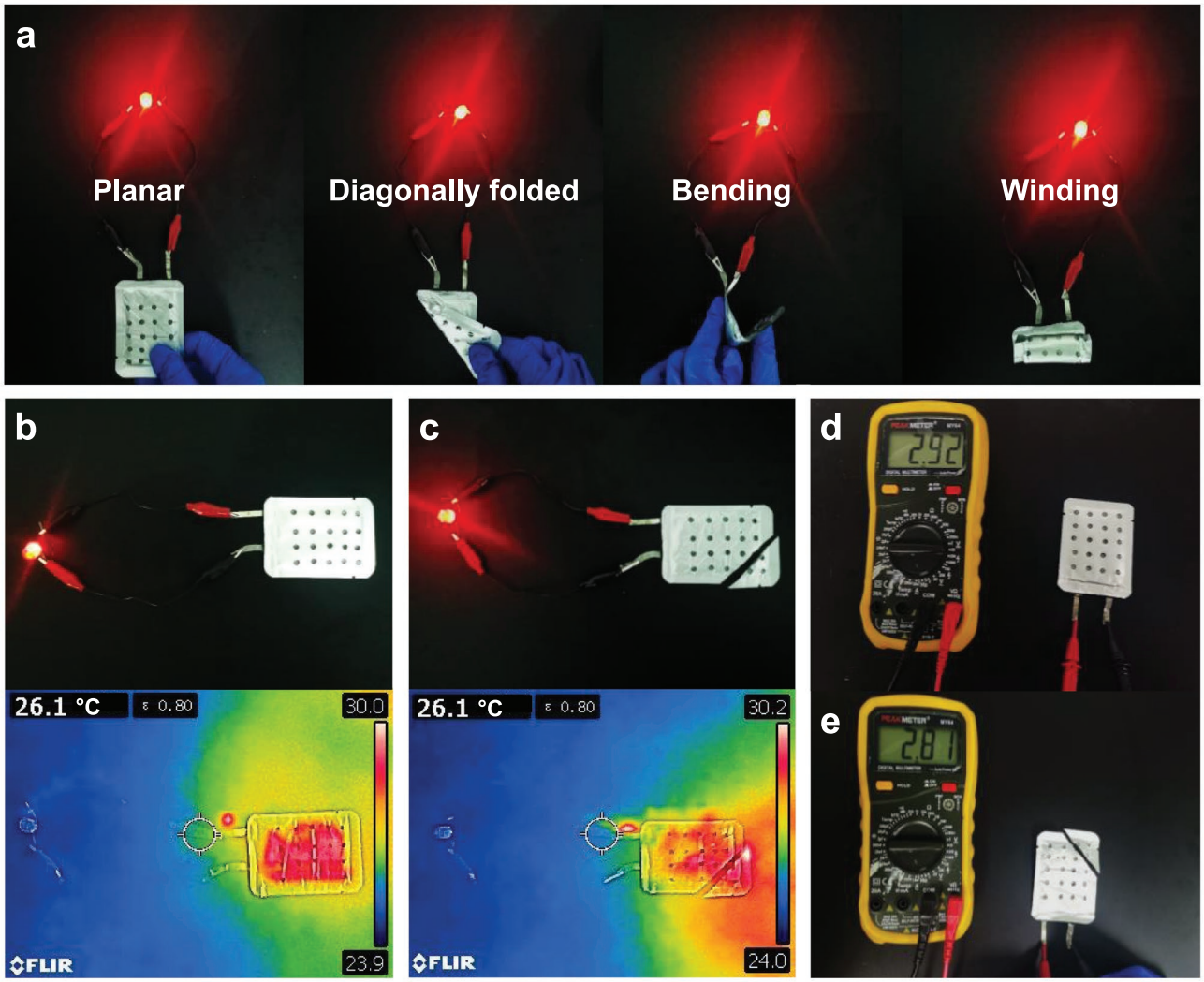

Figure 5. The flexibility and safety tests of the pouch-type SSLOBs. a) Photographs of the pouch-type SSLOB powering an LED light under planar, diagonally folded, bending, and winding states. Photographs and corresponding infrared thermal images of the pouch-type SSLOB b) before and c) after cut test. Open circuit voltages of the pouch-type SSLOB d) before and e) after cut test.

those of the literature reported values (Figure 3f).[32–40] The preliminary data presented here implies the great potential of the SiO_2 NFs framework supported ICES in promoting the practical application of SSLOBs.

The electrochemical reactions happened in the ICES-based SSLOB were then investigated by characterizing the discharged and recharged cathodes. As can be seen from the SEM images in **Figure 4**a,b, some particulate discharge products are dispersed on the surface of the discharged cathode, and these discharge products disappear and the cathode almost reverts back to the original state after subsequent recharge process. The composition of the discharge products was then analyzed by XRD. There are clear peaks corresponding to the Li_2O_2 phase for the discharged cathode, and the Li_2O_2 subsequently vanish after charging (Figure 4c), indicating the reversible formation and decomposition of Li_2O_2. These results demonstrate that the ICES-based SSLOBs follow the typical O_2 and Li_2O_2 conversion reactions with good reversibility. In addition, the Li anode protection ability of the ICES in the rigorous working environment of SSLOBs was examined. SEM images show that the cycled Li anode surface remains flat and smooth (Figure 4d,e), demonstrating that the CSE side in the ICES could effectively protect the Li anode from corrosion and dendrite growth. Moreover, the inconspicuous LiOH peaks in the cycled Li anode further confirm this kind of anode protection ability enabled by the ICES (Figure 4f).

Considering the flexible and free-standing feature of the ICES, pouch-type SSLOBs were assembled by just pairing the ICES with the Li sheet, which simplifies the assembly processes compared with the conventional SSLOBs. The prepared pouch-type SSLOB can power the red light-emitting diode (LED) light under planar, diagonally folded, bending, and winding states, signifying the excellent flexibility of the ICES-based SSLOBs for practical application (**Figure 5**a). To investigate the safety of the ICES-based SSLOBs, nail penetration and cutting-corner tests were conducted. After nail penetration, the pouch-type SSLOBs

can still power the red LED light, and the temperature of the cell almost experiences no change, not to mention the occurrence of fire or explosion (Figure S13, Supporting Information). Importantly, even cutting off one corner of the pouch-type SSLOB, the cell still does not display any signs of short-circuit or fire (Figure 5b,c), and the red LED light can still be normally powered by the dissected cell. Infrared thermal images show that the temperature at the cut corner is slightly higher than other places, but the overall temperature of the cell is below 30.2 °C. Furthermore, after cutting off the corner, the cell could still maintain a high open-circuit voltage of 2.81 V (Figure 5d,e). The outstanding security of the ICES-based SSLOBs can be ascribed to the replacement of the flammable organic liquid electrolyte with ICES, avoiding the risk of leakage and fire hazards.

3. Conclusion

In summary, a flexible and free-standing ICES for SSLOBs has been designed by supporting the cathode material and polymer electrolyte on an elaborately engineered 3D SiO_2 NFs framework. In the integrated structure, the ceramic framework enables the firm contact between the cathode and electrolyte, and acts as a 3D ceramic filler for the polymer electrolyte and a matrix for the porous cathode, thus decreasing the interfacial resistance, improving the Li^+ conductivity of the polymer electrolyte, and increasing the reaction sites in the cathode side. As a result, the three key challenges that limit the high-performance operation of SSLOBs are conquered, making the batteries deliver high discharge capacity, rate performance, and long cycle lifetime (145 cycles). This work provides a new concept and direction for the design and development of high-performance, flexible, and safe SSLOBs.

Supporting Information

Supporting Information is available from the Wiley Online Library or from the author.

Acknowledgements

C.-L.L. and G.H. contributed equally to this work. This work was financially supported by the National Key R&D Program of China (Grant 2017YFA0206704), National Natural Science Foundation of China (Grant 21725103), Jilin Province Science and Technology Development Plan Funding Project (Grant 20200201079JC), and Key Research Program of the Chinese Academy of Sciences (Grant ZDRW-CN-2021-3).

Conflict of Interest

The authors declare no conflict of interest.

Data Availability Statement

The data that support the findings of this study are available from the corresponding author upon reasonable request.

Keywords

composite solid electrolytes, integrated structures, SiO_2 nanofibers frameworks, solid-state lithium–oxygen batteries

Received: December 16, 2021
Revised: March 6, 2022
Published online:

[1] D. Aurbach, B. D. McCloskey, L. F. Nazar, P. G. Bruce, *Nat. Energy* **2016**, *1*, 16128.
[2] M. Asadi, B. Sayahpour, P. Abbasi, A. T. Ngo, K. Karis, J. R. Jokisaari, C. Liu, B. Narayanan, M. Gerard, P. Yasaei, X. Hu, A. Mukherjee, K. C. Lau, R. S. Assary, F. Khalili-Araghi, R. F. Klie, L. A. Curtiss, A. Salehi-Khojin, *Nature* **2018**, *555*, 502.
[3] P. G. Bruce, S. A. Freunberger, L. J. Hardwick, J. M. Tarascon, *Nat. Mater.* **2012**, *11*, 19.
[4] S. Choudhury, C. T. Wan, W. I. Al Sadat, Z. Tu, S. Lau, M. J. Zachman, L. F. Kourkoutis, L. A. Archer, *Sci. Adv.* **2017**, *3*, e1602809.
[5] J. J. Xu, Q. C. Liu, Y. Yu, J. Wang, J. M. Yan, X. B. Zhang, *Adv. Mater.* **2017**, *29*, 1606552.
[6] F. Liu, Q. Xiao, H. B. Wu, L. Shen, D. Xu, M. Cai, Y. Lu, *Adv. Energy Mater.* **2018**, *8*, 1701744.
[7] X.-B. Cheng, C. Yan, X. Chen, C. Guan, J.-Q. Huang, H.-J. Peng, R. Zhang, S.-T. Yang, Q. Zhang, *Chem* **2017**, *2*, 258.
[8] S. Xia, X. Wu, Z. Zhang, Y. Cui, W. Liu, *Chem* **2019**, *5*, 753.
[9] J. Wan, J. Xie, X. Kong, Z. Liu, K. Liu, F. Shi, A. Pei, H. Chen, W. Chen, J. Chen, X. Zhang, L. Zong, J. Wang, L. Q. Chen, J. Qin, Y. Cui, *Nat. Nanotechnol.* **2019**, *14*, 705.
[10] X. Chi, M. Li, J. Di, P. Bai, L. Song, X. Wang, F. Li, S. Liang, J. Xu, J. Yu, *Nature* **2021**, *592*, 551.
[11] N. Zhao, W. Khokhar, Z. Bi, C. Shi, X. Guo, L.-Z. Fan, C.-W. Nan, *Joule* **2019**, *3*, 1190.
[12] L. Fan, S. Wei, S. Li, Q. Li, Y. Lu, *Adv. Energy Mater.* **2018**, *8*, 1702657.
[13] W. Liu, C. Yi, L. Li, S. Liu, Q. Gui, D. Ba, Y. Li, D. Peng, J. Liu, *Angew. Chem., Int. Ed.* **2021**, *60*, 12931.
[14] W. Liu, S. W. Lee, D. Lin, F. Shi, S. Wang, A. D. Sendek, Y. Cui, *Nat. Energy* **2017**, *2*, 17035.
[15] F. Croce, G. B. Appetecchi, L. Persi, B. Scrosati, *Nature* **1998**, *394*, 456.
[16] J. Zhang, N. Zhao, M. Zhang, Y. Li, P. K. Chu, X. Guo, Z. Di, X. Wang, H. Li, *Nano Energy* **2016**, *28*, 447.
[17] L. Yang, Z. Wang, Y. Feng, R. Tan, Y. Zuo, R. Gao, Y. Zhao, L. Han, Z. Wang, F. Pan, *Adv. Energy Mater.* **2017**, *7*, 1701437.
[18] D. Lin, P. Y. Yuen, Y. Liu, W. Liu, N. Liu, R. H. Dauskardt, Y. Cui, *Adv. Mater.* **2018**, *30*, 1802661.
[19] K. K. Fu, Y. Gong, J. Dai, A. Gong, X. Han, Y. Yao, C. Wang, Y. Wang, Y. Chen, C. Yan, Y. Li, E. D. Wachsman, L. Hu, *Proc. Natl. Acad. Sci. USA* **2016**, *113*, 7094.
[20] J. Bae, Y. Li, J. Zhang, X. Zhou, F. Zhao, Y. Shi, J. B. Goodenough, G. Yu, *Angew. Chem., Int. Ed.* **2018**, *57*, 2096.
[21] H. Xie, C. Yang, K. K. Fu, Y. Yao, F. Jiang, E. Hitz, B. Liu, S. Wang, L. Hu, *Adv. Energy Mater.* **2018**, *8*, 1703474.
[22] X. Chen, W. He, L.-X. Ding, S. Wang, H. Wang, *Energy Environ. Sci.* **2019**, *12*, 938.
[23] Z. Chang, J. Xu, X. Zhang, *Adv. Energy Mater.* **2017**, *7*, 1700875.
[24] X. B. Zhu, T. S. Zhao, Z. H. Wei, P. Tan, G. Zhao, *Energy Environ. Sci.* **2015**, *8*, 2782.
[25] H. Kitaura, H. Zhou, *Adv. Energy Mater.* **2012**, *2*, 889.
[26] L. Wang, Y. Qiu, H. Lv, Y. Si, L. Liu, Q. Zhang, J. Cao, J. Yu, X. Li, B. Ding, *Adv. Funct. Mater.* **2019**, *29*, 1901407.

[27] Y. Si, L. Wang, X. Wang, N. Tang, J. Yu, B. Ding, *Adv. Mater.* **2017**, *29*, 1700339.
[28] P. Martins, A. C. Lopes, S. Lanceros-Mendez, *Prog. Polym. Sci.* **2014**, *39*, 683.
[29] D. Chen, Z. Zhou, C. Feng, W. Lv, Z. Wei, K. H. L. Zhang, B. Lin, S. Wu, T. Lei, X. Guo, G. Zhu, X. Jian, J. Xiong, E. Traversa, S. X. Dou, W. He, *Adv. Energy Mater.* **2019**, *9*, 1803627.
[30] H. Yang, J. Bright, B. Chen, P. Zheng, X. Gao, B. Liu, S. Kasani, X. Zhang, N. Wu, *J. Mater. Chem. A* **2020**, *8*, 7261.
[31] W. Liu, N. Liu, J. Sun, P. C. Hsu, Y. Li, H. W. Lee, Y. Cui, *Nano Lett.* **2015**, *15*, 2740.
[32] Y. Liu, C. Li, B. Li, H. Song, Z. Cheng, M. Chen, P. He, H. Zhou, *Adv. Energy Mater.* **2018**, *8*, 1702374.
[33] J. Sun, N. Zhao, Y. Li, X. Guo, X. Feng, X. Liu, Z. Liu, G. Cui, H. Zheng, L. Gu, H. Li, *Sci. Rep.* **2017**, *7*, 41217.
[34] W. Yu, C. Xue, B. Hu, B. Xu, L. Li, C.-W. Nan, *Energy Storage Mater.* **2020**, *27*, 244.
[35] H. Kitaura, H. Zhou, *Sci. Rep.* **2015**, *5*, 13271.
[36] Y. Liu, B. Li, Z. Cheng, C. Li, X. Zhang, S. Guo, P. He, H. Zhou, *J. Power Sources* **2018**, *395*, 439.
[37] Y. Liu, B. Li, H. Kitaura, X. Zhang, M. Han, P. He, H. Zhou, *ACS Appl. Mater. Interfaces* **2015**, *7*, 17307.
[38] S. Wang, J. Wang, J. Liu, H. Song, Y. Liu, P. Wang, P. He, J. Xu, H. Zhou, *J. Mater. Chem. A* **2018**, *6*, 21248.
[39] X. Wang, D. Zhu, M. Song, S. Cai, L. Zhang, Y. Chen, *ACS Appl. Mater. Interfaces* **2014**, *6*, 11204.
[40] X. Wang, S. Cai, D. Zhu, Y. Chen, *RSC Adv.* **2015**, *5*, 88485.